Research Article
Experimental and Translational Hepatology

JOURNAL
OF HEPATOLOGY

PKCα/ZFP64/CSF1 axis resets the tumor microenvironment and fuels anti-PD1 resistance in hepatocellular carcinoma

Graphical abstract

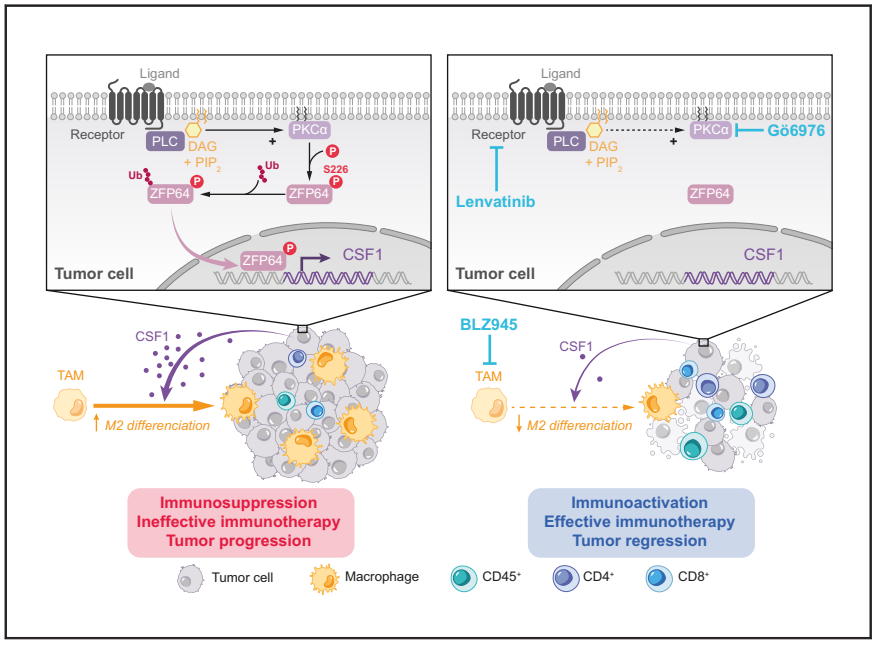

Highlights

- ZFP64 is frequently upregulated in anti-PD1 resistant HCC.
- PKCα/ZFP64/CSF1 axis is critical for triggering immune evasion and anti-PD1 tolerance.
- Gö6976 and lenvatinib overcome anti-PD1 resistance by blocking the PKCα/ZFP64/CSF1 axis.
- Gö6976 combined with anti-PD1 could be an effective new strategy in HCC therapy.

Authors

Chuan-Yuan Wei, Meng-Xuan Zhu, Peng-Fei Zhang, …, Jia-Bin Fan, Ai-Wu Ke, Jia Fan

Correspondence

fan.jia@zs-hospital.sh.cn (J. Fan), ke.aiwu@zs-hospital.sh.cn (A.-W. Ke), cai.jiabin@zs-hospital.sh.cn (J.-B. Fan).

Lay summary

Despite remarkable treatment progress, most patients with hepatocellular carcinoma respond poorly to anti-PD1 therapy (a type of immunotherapy). A deeper insight into the tolerance mechanisms to this therapy is urgently needed. Herein, we unravel a previously unexplored mechanism linking tumor progression, macrophage polarization, and anti-PD1 resistance, and offer an attractive novel target for anti-PD1 combination therapy, which may benefit patients with hepatocellular carcinoma.

https://doi.org/10.1016/j.jhep.2022.02.019
 J. Hepatol. 2022, 77, 163–176

Research Article
Experimental and Translational Hepatology

JOURNAL OF HEPATOLOGY

PKCα/ZFP64/CSF1 axis resets the tumor microenvironment and fuels anti-PD1 resistance in hepatocellular carcinoma

Chuan-Yuan Wei[1,2,#], Meng-Xuan Zhu[3,#], Peng-Fei Zhang[3,#], Xiao-Yong Huang[1], Jin-Kai Wan[4], Xiu-Zhong Yao[5], Ze-Tao Hu[6], Xiao-Qiang Chai[1], Rui Peng[1], Xuan Yang[1], Chao Gao[1], Jian Gao[1], Si-Wei Wang[1], Yi-Min Zheng[1], Zheng Tang[1], Qiang Gao[1], Jian Zhou[1], Jia-Bin Fan[1,*], Ai-Wu Ke[1,*], Jia Fan[1,*]

[1]*Department of Liver Surgery and Transplantation, Key Laboratory of Carcinogenesis and Cancer Invasion (Ministry of Education), Liver Cancer Institute, Zhongshan Hospital, Fudan University, Shanghai, 200032, P. R. China;* [2]*Department of Plastic Surgery, Zhongshan Hospital, Fudan University, Shanghai, 200032, P. R. China;* [3]*Department of Medical Oncology, Zhongshan Hospital, Fudan University, Shanghai, 200032, P. R. China;* [4]*Shanghai Key Laboratory of Medical Epigenetics, International Co-laboratory of Medical Epigenetics and Metabolism, Ministry of Science and Technology, Institutes of Biomedical Sciences, Fudan University, Shanghai, 200032, P. R. China;* [5]*Department of Radiology, Zhongshan Hospital of Fudan University, Fudan University, Shanghai Institute of Medical Imaging, Shanghai, 200032, P. R. China;* [6]*Department of Biochemistry, School of Life Sciences, Fudan University, Shanghai, 200433, P. R. China*

See Editorial, pages 9–11

Background & Aims: Despite remarkable advances in treatment, most patients with hepatocellular carcinoma (HCC) respond poorly to anti-programmed cell death 1 (anti-PD1) therapy. A deeper insight into the tolerance mechanism of HCC against this therapy is urgently needed.

Methods: We performed next-generation sequencing, multiplex immunofluorescence, and dual-color immunohistochemistry and constructed an orthotopic HCC xenograft tumor model to identify the key gene associated with anti-PD1 tolerance. A spontaneously tumorigenic transgenic mouse model, an *in vitro* coculture system, mass cytometry, and multiplex immunofluorescence were used to explore the biological function of zinc finger protein 64 (ZFP64) on tumor progression and immune escape. Molecular and biochemical strategies like RNA-sequencing, chromatin immunoprecipitation-sequencing and mass spectrometry were used to gain insight into the underlying mechanisms of ZFP64.

Results: We showed that ZFP64 is frequently upregulated in tumor tissues from patients with anti-PD1-resistant HCC. Elevated ZFP64 drives anti-PD1 resistance by shifting macrophage polarization toward an alternative activation phenotype (M2) and fostering an inhibitory tumor microenvironment. Mechanistically, we primarily demonstrated that protein kinase C alpha (PKCα) directly phosphorylates ZFP64 at S226, leading to its nuclear translocation and the transcriptional activation of macrophage colony-stimulating factor (CSF1). HCC-derived CSF1 transforms macrophages to the M2 phenotype to drive immune escape and anti-PD1 tolerance. Notably, Gö6976, a protein kinase inhibitor, and lenvatinib, a multi-kinase inhibitor, reset the tumor microenvironment and restore sensitivity to anti-PD1 by blocking the PKCα/ZFP64/CSF1 axis.

Conclusions: We propose that the PKCα/ZFP64/CSF1 axis is critical for triggering immune evasion and anti-PD1 tolerance. Inhibiting this axis with Gö6976 or lenvatinib overcomes anti-PD1 resistance in HCC.

Lay summary: Despite remarkable treatment progress, most patients with hepatocellular carcinoma respond poorly to anti-PD1 therapy (a type of immunotherapy). A deeper insight into the tolerance mechanisms to this therapy is urgently needed. Herein, we unravel a previously unexplored mechanism linking tumor progression, macrophage polarization, and anti-PD1 resistance, and offer an attractive novel target for anti-PD1 combination therapy, which may benefit patients with hepatocellular carcinoma.

Introduction

Hepatocellular carcinoma (HCC) is one of the most prevalent and life-threatening malignancies globally, and a considerable proportion of patients with HCC are diagnosed at advanced stages and, therefore, cannot undergo curative surgery.[1,2] Recently, immune checkpoint blockade (ICB) therapy, especially with antibodies against the programmed cell death (/ligand) 1 (PD1/PD-L1) signal, has led to impressive breakthroughs in cancer treatment.[3] However, randomized clinical trials of anti-PD1 therapy (KEYNOTE-240 and CheckMate-459) in patients with HCC have not shown statistically significant improvements, potentially owing to primary or acquired anti-PD1 resistance.[4,5] There is an urgent need to explore mechanisms of resistance to ICB therapy, and identify a combined therapeutic strategy to enhance the effectiveness of ICB therapy in HCC.

Keywords: zinc finger protein 64; anti-PD1 resistance; tumor microenvironment; phosphorylation modification; combination therapy.
Received 26 September 2021; received in revised form 28 January 2022; accepted 9 February 2022; available online 24 February 2022

* Corresponding authors. Address: Department of Liver Surgery and Transplantation, Key Laboratory of Carcinogenesis and Cancer Invasion (Ministry of Education), Liver Cancer Institute, Zhongshan Hospital, Fudan University, Shanghai, 200032, P. R. China
E-mail addresses: fan.jia@zs-hospital.sh.cn (J. Fan), ke.aiwu@zs-hospital.sh.cn (A.-W. Ke), cai.jiabin@zs-hospital.sh.cn (J.-B. Fan).
# These authors contributed equally.

https://doi.org/10.1016/j.jhep.2022.02.019

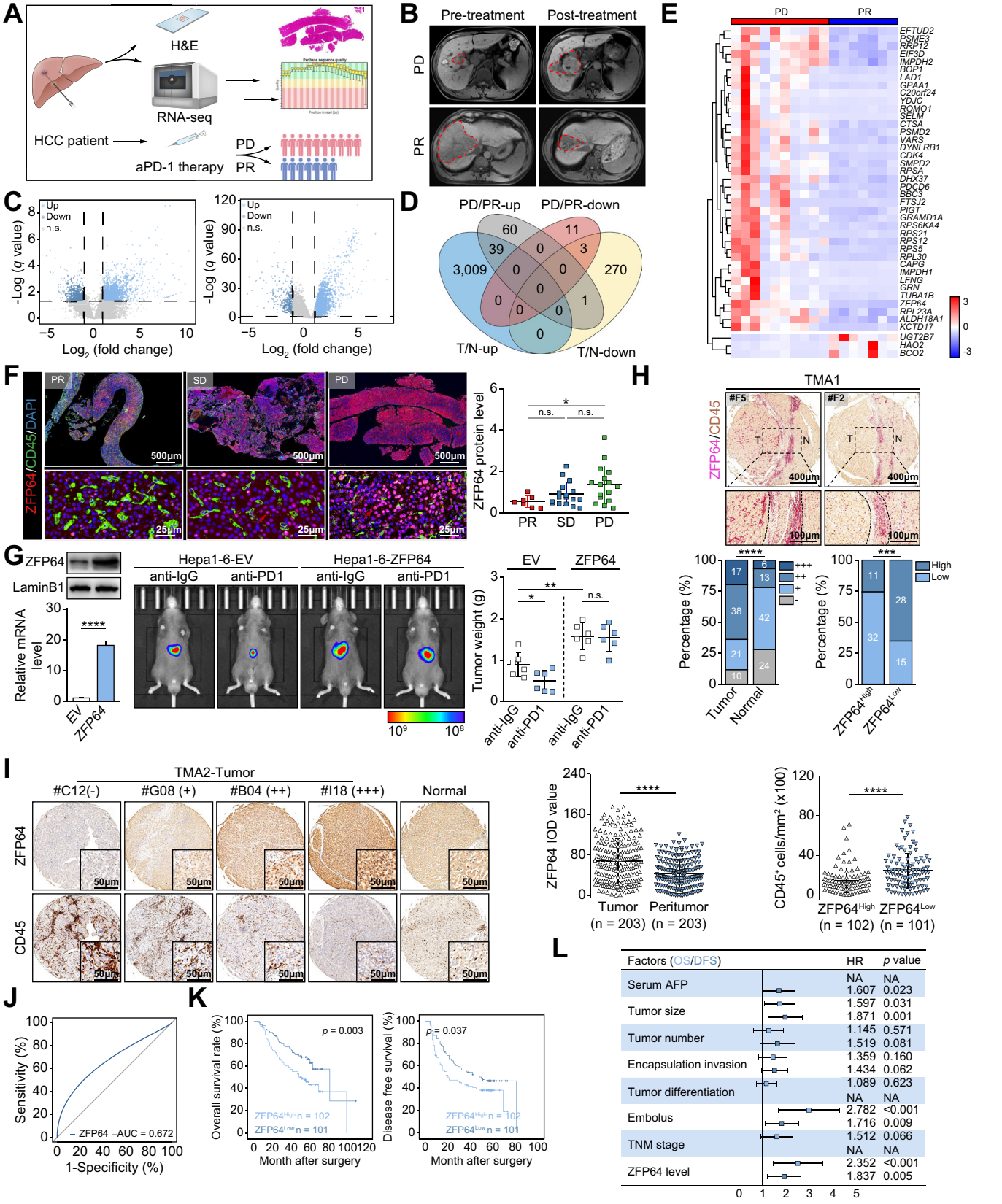

Fig. 1. ZFP64 is tightly correlated with anti-PD1 monotherapy tolerance and poor prognosis in patients with HCC. (A) Schematic diagram of the recruitment of patients and specimens in the training cohort. (B) Representative MRIs of patients with PD and PR. (C) Volcano plots showing DEGs in the training (PD *vs.* PR, left panel) and TCGA-LIHC (T *vs.* N, right panel) cohorts. |log2FC| > 1, q-value <0.05. (D) Venn diagram showing an overlap of DEGs between the 2 cohorts. (E) Heatmap showing the overlapping genes in the Venn diagram. (F) Representative images of ZFP64 protein detection using IF assays. Red arrows (ZFP64$^+$ cells), green arrows (CD45$^+$ cells). (G)

As an immune-exempt organ, the liver contains a large number of macrophages, including resident (Kupffer cells) and recruited macrophages.[6] Macrophages that infiltrate tumor tissues, also known as tumor-associated macrophages (TAMs), are functionally and phenotypically similar to alternately activated (M2-like) macrophages, and play an important role in tumor progression, immune escape and ICB therapy resistance.[7–9] Several studies have uncovered the marked effect of TAMs on the efficacy of ICB therapy. For example, a unique population of macrophages highly expressing CD73 was reported to persist during anti-PD1 treatment, and consecutive CD73 knockout improved the efficacy of anti-PD1 therapy.[10] Thus, reversing the M2 phenotype, blocking the recruitment of TAMs, and stopping TAMs infiltration are expected to be effective strategies to improve the efficacy of ICB therapy in HCC.

The zinc finger protein 64 (ZFP64) gene, located at 20q13.2, was identified as a new Kruppel-like C2H2 transcriptional factor.[11] The amplification of genes in the 20q13.12–13.33 locus was reported to be associated with increased metastasis and reduced overall survival (OS) in patients with HCC.[12] Meanwhile, ZFP64 was revealed to be upregulated in liver metastatic tissues of colorectal carcinoma.[13] A recent study has shown that ZFP64 is necessary for the continuous expression of mixed-lineage leukemia (MLL) fusion proteins, and ZFP64 knockout completely inhibited leukemic cell proliferation.[14] These findings indicate that abnormal ZFP64 expression plays a key role in tumor development.

Here, we aimed to identify differentially expressed genes (DEGs) associated with anti-PD1 tolerance via next-generation sequencing. We identified crucial genes/pathways and a mechanism of the anti-PD1 tolerance in HCC that involves ZFP64, its upstream regulator, and its downstream effector. Our findings primarily demonstrated a previously unexplored mechanism linking tumor anti-PD1 tolerance, provided a predictive indicator for monitoring anti-PD1 efficacy, and offered a potential combination strategy against HCC.

Materials and methods

Details regarding the materials and methods are described in the supplementary information. Reagents used in this study are listed in the CTAT table.

Results

ZFP64 is a crucial gene associated with anti-PD1 tolerance and unfavorable prognosis in patients with HCC

We performed next-generation sequencing to analyze biopsy specimens from patients with HCC scheduled to receive anti-PD1 therapy (Fig. 1A). The treatment efficacy was monitored by MRI bimonthly (Fig. 1B), and assessed according to iRECIST.[15] A total of 41 patients were recruited, and the objective response and disease control rates were 17.1% and 61.0%, respectively (Table S1, discovery cohort). Ten progressive disease (PD) and 7 partial response (PR) samples were selected for sequencing and 2,090 DEGs (PD *vs.* PR, Fig. 1C, left panel) were identified. Of note, immune checkpoint molecules, such as PD1, PD-L1, and PD-L2, were not included (Fig. S1A). Then we performed an intersection of DEGs in the discovery cohort and The Cancer Genome Atlas (TCGA) cohort (tumor *vs.* normal, Fig. 1C, right panel), and 39 upregulated and 3 downregulated genes were identified, as illustrated in Fig. 1D-E.

ZFP64, one of the upregulated genes, was selected for further study.[14,16] In the discovery cohort, ZFP64, primarily in the nucleus, was consistently increased in PD samples compared to that in SD or PR samples (Fig. 1F), while CD45-positive immune cells were decreased in the TIME of PD samples. Using an orthotopic xenograft tumor model, we found that the tumor burden in the ZFP64-overexpressing group (Hepa1-6-ZFP64) was larger than that in the empty vector (EV) group (Hepa1-6-EV) (Fig. 1G). Notably, the tumor burden in the Hepa1-6-EV group was significantly decreased after anti-PD1 treatment compared with that after anti-IgG treatment, whereas no statistical difference was observed in Hepa1-6-ZFP64 groups.

In the TCGA cohort, ZFP64 expression was significantly elevated in HCC, and the AUROC was 0.903 (Fig. S1B–D). We performed immunoblotting of HCC samples and found that ZFP64 was upregulated in tumor tissues compared to normal tissues (Fig. S1E). In validation cohorts (TMA1 and TMA2), ZFP64 levels were significantly increased in HCC tumor tissues compared to in normal tissues, and elevated ZFP64 levels were often accompanied by less lymphocyte infiltration in the TIME (Fig. 1H-I). The AUROC of ZFP64 was demonstrated to be 0.692 (Fig. 1J).

Prognostic analysis showed that elevated ZFP64 correlated with malignant phenotype and poor prognosis in patients with HCC in the TCGA and TMA2 cohorts (Fig. 1K and S1F, Table S2). Importantly, multivariate logistic regression analyses showed that highs level of ZFP64 were independent predictors for postoperative OS and disease-free survival (Fig. 1L, Table S3). Thus, ZFP64 is a key gene associated with poor prognosis and anti-PD1 resistance in HCC.

ZFP64 promotes HCC progression and induces an inhibitory TIME

We then explored the function of ZFP64 in HCC. ZFP64 was highly expressed in HCC cell lines, especially those with high metastatic potential (Fig. S2A–B). We then generated the stable *ZFP64*-knockout (single-guide *ZFP64*) MHCC97H and *ZFP64*-overexpressing PLC/PRF/5 and HepG2 cell lines (Fig. S2C–F), and found that cell proliferation, motility, and invasion abilities were increased in ZFP64^{high} cells compared with those in ZFP64^{low} cells (Fig. S3A–B). By employing subcutaneous xenograft tumor models, we found that ZFP64^{high} groups have higher tumor weights and fewer apoptotic cells than ZFP64^{low} groups (Fig. S3C–D).

Immunoblotting and qRT-PCR assays showing the efficiency of ZFP64 overexpression. Bioluminescence images of HCC tumors in C57BL/6 mice are shown at the endpoint. The color scale bar depicts the photon flux emitted from tumors. Tumor weight data were analyzed statistically (n = 6). (H) Double IHC staining with ZFP64-specific and CD45-specific antibodies in TMA1 (upper panel). Percentage of cases were analyzed by ZFP64 expression (bottom left panel) or CD45^{+} lymphocyte number (bottom right). -, negative; +, low; ++, moderate; +++, strong. (I) IHC staining with ZFP64-specific and CD45-specific antibodies to detect ZFP64 expression and CD45^{+} lymphocyte infiltration in TMA2. (J) The AUROC for distinguishing HCC tumors from normal tissues. (K) OS and DFS curves based on ZFP64 expression using the Kaplan–Meier method and analyzed by log-rank test. (L) Forest plot showing the results of multivariate analysis of factors associated with OS and DFS. DFS, disease-free survival; HCC, hepatocellular carcinoma; IF, immunofluorescence; IHC, immunohistochemistry; N, normal; OS, overall survival; PD, progressive disease; PR, partial response; qRT-PCR, quantitative reverse-transcription PCR; T, tumor. (This figure appears in color on the web.)

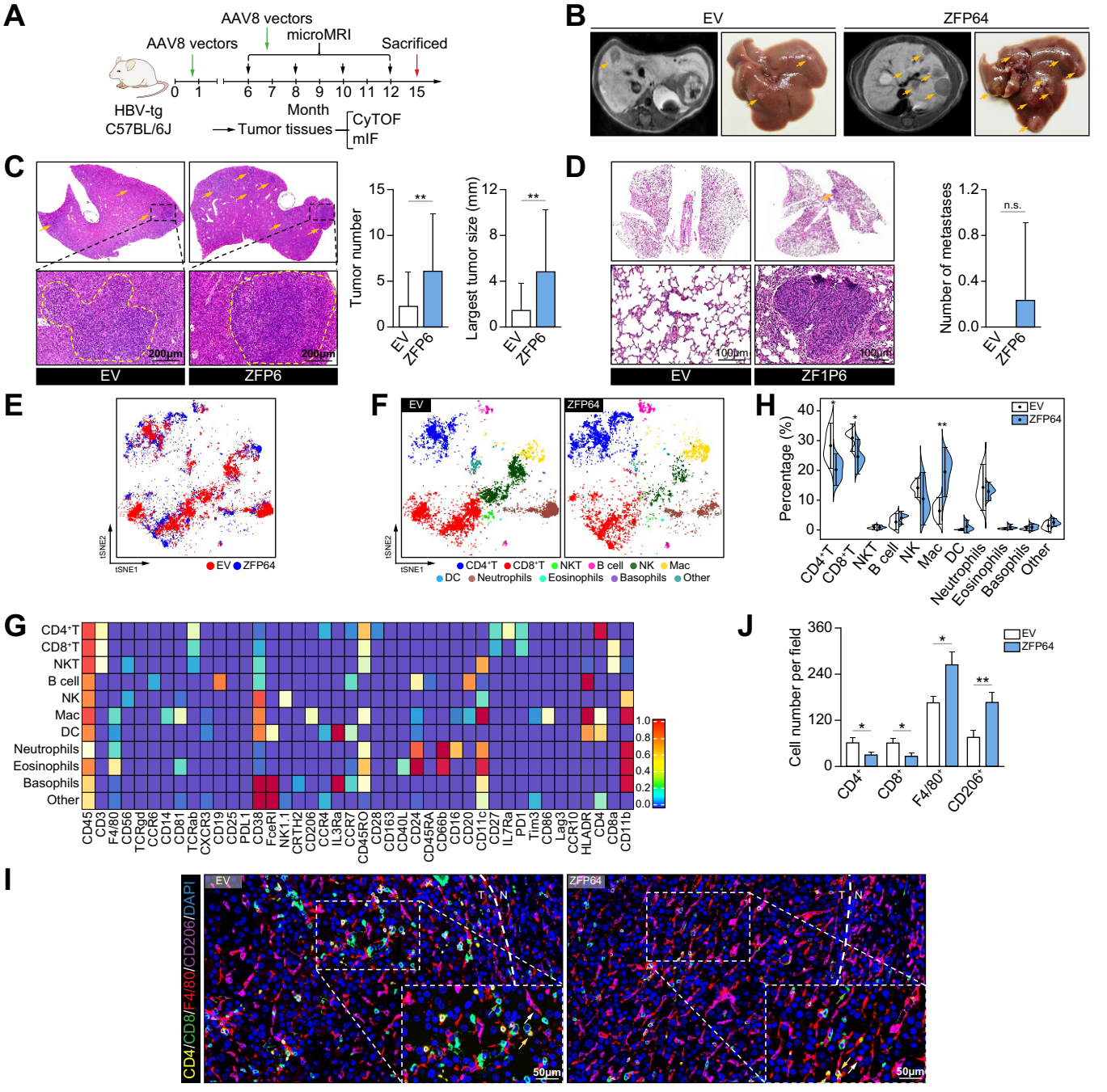

Fig. 2. ZFP64 accelerates tumor progression and induces a suppressive TIME. (A) Workflow of the spontaneous HCC model. Hepatic ZFP64 overexpression following injection of AAV8 vectors into the tail vein of transgenic mice. Sixty mice were randomly divided into 2 groups. (B) Periodical detection of tumor development and progression using microMRI; representative images are presented at the endpoint. Tumor sites are indicated by yellow arrows. (C-D) Tumor sites in livers (C) and lungs (D) were detected by H&E staining, and indicated by yellow arrows. (E-F) t-SNE analysis of CyTOF data of immune cells from tumor tissues. (G) The heatmap showing the expression of target proteins in all 11 subclusters. (H) Violin plots representing the quantification of tumor-infiltrating immune cells. (I) Representative pictures of mIF analysis for CD4 (yellow arrows), CD8 (green arrows), F4/80 and CD206 (white arrows) markers. (J) Quantification of corresponding immune cells by mIF analysis. AAV8, adeno-associated virus serotype 8; CyTOF, mass cytometry by time of flight; HCC, hepatocellular carcinoma; mIF, multiplex immunofluorescence; TIME, tumor immune microenvironment; t-SNE, t-distributed stochastic neighbor embedding. (This figure appears in color on the web.)

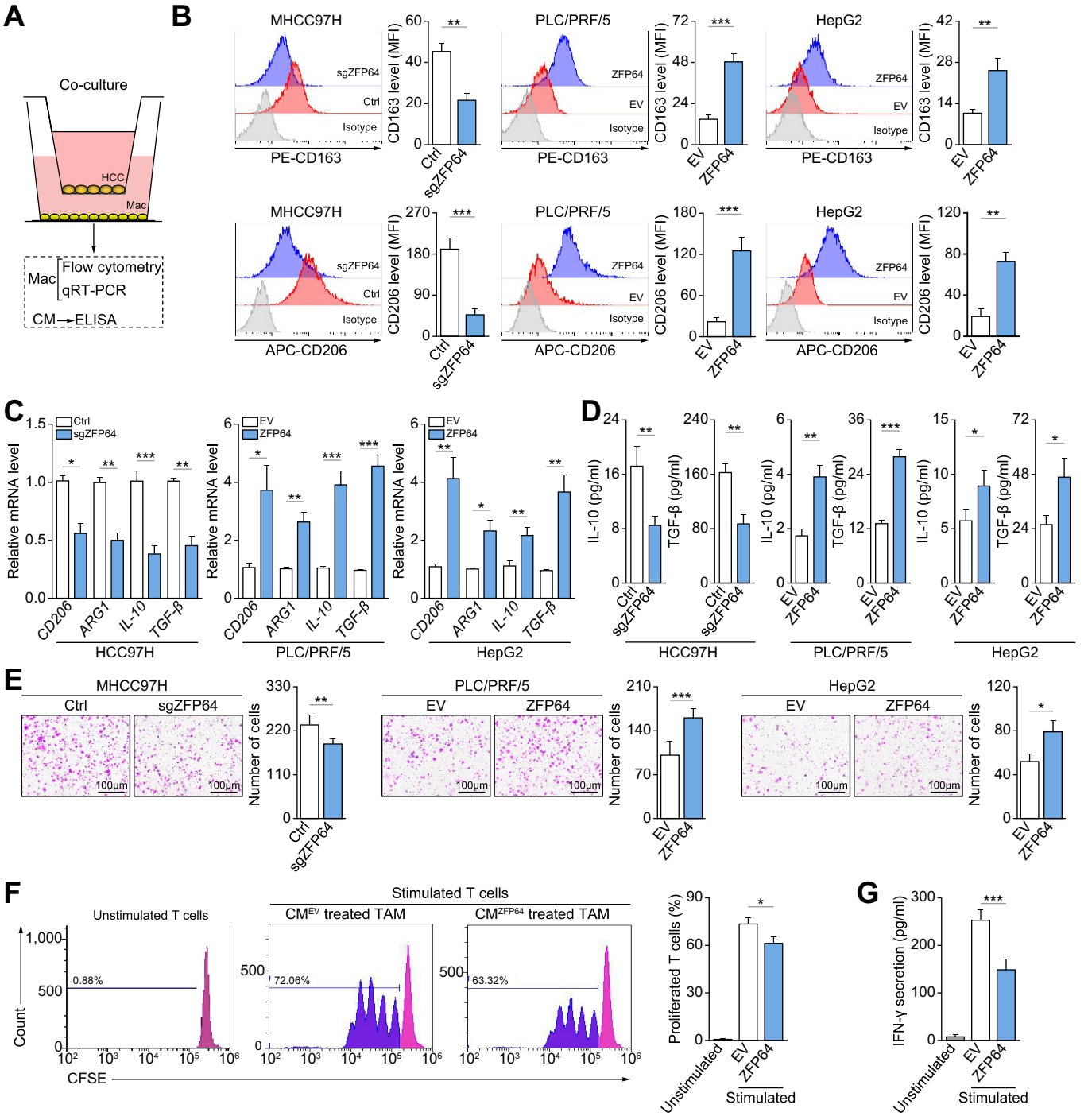

Fig. 3. HCC-expressing ZFP64 induces recruitment and M2 polarization of macrophages. (A) Schematic diagram showing HCC cells cocultured with macrophages using a 0.4-μm pore size Transwell system. (B) CD163 and CD206 expression in macrophages detected by FCM. (C) *CD206*, *ARG1*, *IL-10*, and *TGF-β* mRNA levels in macrophages detected by qRT-PCR. (D) Secreted IL-10 and TGF-β in the supernatants of macrophages detected by ELISA. (E) Chemotactic migration assays of macrophages using the supernatant of PLC/PRF/5-EV or -ZFP64 cells. (F) CFSE histograms detecting the inhibition of T-cell proliferation by macrophages after treatment with the supernatant of PLC/PRF/5-EV or -ZFP64 cells. (G) IFN-γ secretion by CD8+ T cells in the assay in (F), measured by ELISA. FCM, flow cytometry; HCC, hepatocellular carcinoma; qRT-PCR, quantitative reverse-transcription PCR. (This figure appears in color on the web.)

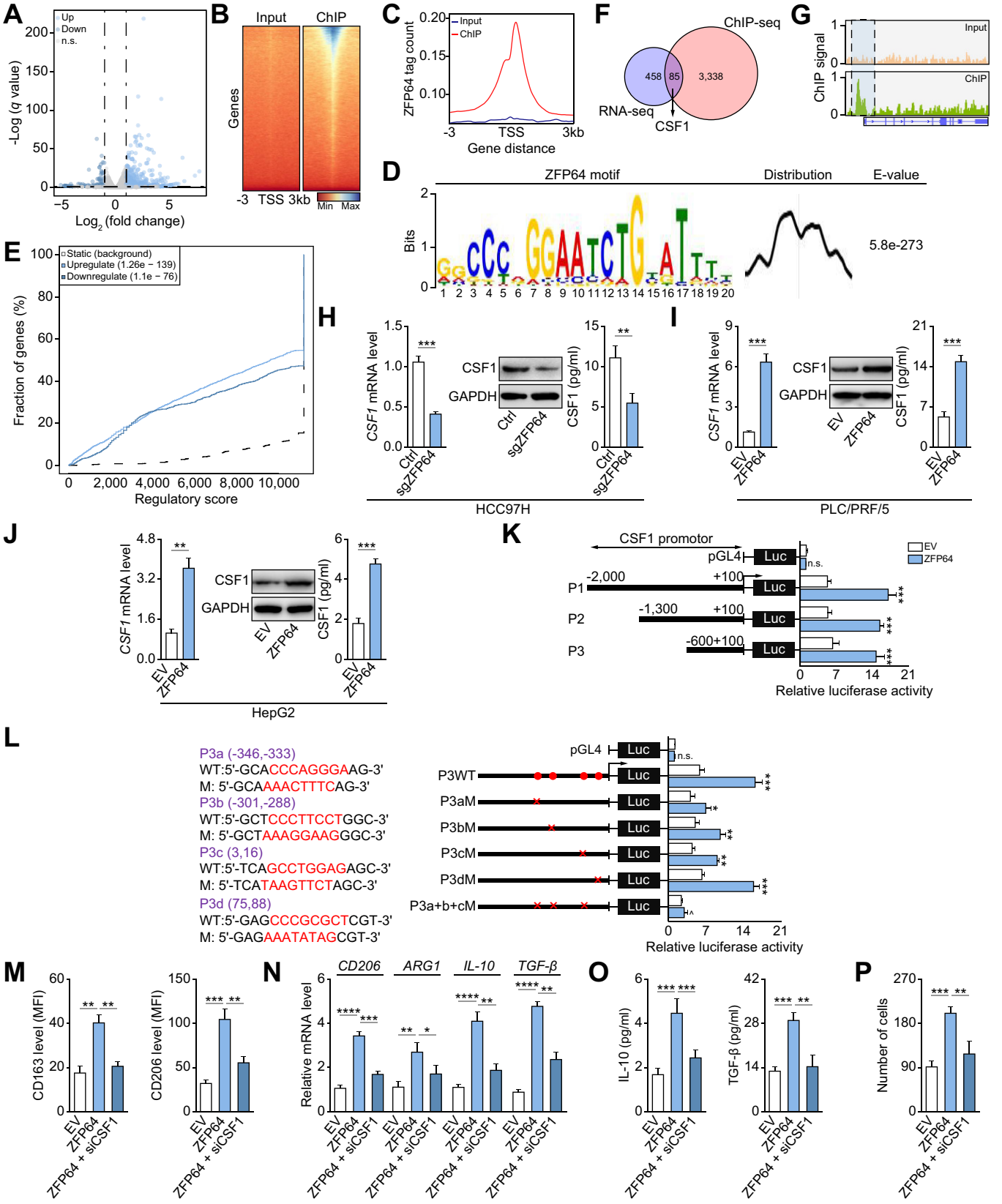

Fig. 4. HCC-expressing ZFP64 promotes macrophage polarization and recruitment via CSF1 transcription. (A) Volcano plot showing DEGs between PLC/PRF/5-ZFP64 and PLC/PRF/5-EV cells. |log2FC| > 1, p-value <0.05. (B–C) Density plot showing the ChIP-sequencing result of high-confidence ZFP64 peaks, ranked by intensity. (D) ZFP64 ChIP-sequencing-derived *de novo* motif logo, distribution, and E-value of the ZFP64 binding motif. (E) BETA plot of combined computational

Then, we employed a spontaneous tumor model in HBV-transgenic mice (Tg[Alb1HBV]44Bri/J) and overexpressed hepatic *ZFP64* using an adeno-associated virus serotype 8 vector (Fig. 2A and S4A–B).[17] When mice were 15 months old, we collected the liver and lung tissues, and found that the ZFP64-overexpressing group showed increased incidences of cirrhosis, tumorigenesis, lung metastasis, larger tumor sizes, more tumor lesions, and fewer apoptotic cells relative to those in the EV group (Fig. 2B–D and S4C-D).

Using mass cytometry by time of flight (CyTOF) and t-distributed stochastic neighbor embedding analysis, the total cell population was divided into 11 subclusters, and macrophages were increased significantly, while $CD8^+$ and $CD4^+$ T cells were decreased in the ZFP64-overexpressing group (Fig. 2E-H). Further analysis showed that the increased macrophages predominantly presented an M2-phenotype (Fig. S4E–F). Multiplex immunofluorescence assay confirmed the results of CyTOF (Fig. 2I–J). Additionally, we developed an orthotopic xenograft tumor model and further confirmed that ZFP64 knockdown delayed tumor progression and improved the tumor microenvironment (Fig. S4G–H). These results indicate that ZFP64 promotes tumor progression and induces a suppressive TIME.

HCC-derived ZFP64 induces recruitment and M2-like polarization of macrophages

Since TAMs are powerful inducers of immunosuppression,[8] we speculated that ZFP64 induced immunosuppression by promoting macrophage polarization and recruitment. Thus, we treated THP1 cells with phorbol-12-myristate-13-acetate (PMA) to differentiate them into macrophages (Fig. 3A). After being cocultured with $ZFP64^{high}$ HCC cells, macrophages expressed high levels of CD163 and CD206 membrane proteins, showed an upregulation of *CD206, ARG-1, IL-10,* and *TGF-β* mRNA, and produced more IL-10 and TGF-β1 (Fig. 3B–D). Using a chemotactic migration assay, we found that $ZFP64^{high}$ HCC cells promoted the chemotactic recruitment of macrophages (Fig. 3E). Moreover, macrophages cocultured with $ZFP64^{high}$ HCC cells strongly suppressed T-cell proliferation and activation compared to those cocultured with $ZFP64^{low}$ HCC cells (Fig. 3F–G). Together, these results suggest that ZFP64-overexpressing HCC cells promote macrophage recruitment and M2-like polarization.

ZFP64 promotes macrophage polarization and recruitment via transcriptional CSF1 activation

To identify targets regulated by ZFP64, we performed RNA-sequencing and chromatin immunoprecipitation (ChIP)-sequencing in PLC/PRF/5 cells (Fig. 4A–C). Using *de novo* motif analysis, we derived a 20-nucleotide sequence motif closely correlated with ZFP64 occupancy (Fig. 4D). Next, we used the binding and expression target analysis (BETA) software to incorporate the ChIP-sequencing and RNA-sequencing data, and found that ZFP64 functioned both as a transcriptional activator and repressor, but more genes appear to be activated (Fig. 4E).

Subsequently, we took an intersection of the RNA-sequencing and ChIP-sequencing data and obtained 85 genes (Fig. 4F). By performing KEGG analysis, we found that elevated ZFP64 was associated with RAS/MAPK, PI3K/AKT, and TGF-β pathways, and confirmed that elevated ZFP64 increased p-AKT and p-ERK1/2 levels by immunoblotting (Fig. S5A–B). Gene ontology analysis revealed that enhanced ZFP64 was related to monocyte/macrophage activation and migration (Fig. S5C), and associated genes are presented using a heatmap (Fig. S5D). The correlation analyses showed that ZFP64 was correlated with most of the genes, including CSF1, in TCGA cohort (Fig. S5E). Using a 102-cytokine array kit, we observed elevated CSF1 in the supernatant of PLC/PRF/5-ZFP64 cells compared with those in PLC/PRF/5-EV cells (Fig. S6A–B). Thus, we infer that CSF1 may be one of the key transcriptional targets (Fig. 4F–G).

Similarly, we confirmed that high levels of CSF1 were present in $ZFP64^{high}$ cells compared with those in $ZFP64^{low}$ cells (Fig. 4H–J). Then we cloned the *CSF1* promoter region into a luciferase reporter plasmid, and found that all the 3 fragments, including P1 (-2,000 to +100), P2 (-1,300 to +100), and P3 (-600 to +100), could activate the luciferase reporter, indicating that the P3 fragment is sufficient for ZFP64-mediated transcriptional activation (Fig. 4K). Using the JASPAR database, we found that the P3 fragment contained 4 putative ZFP64 binding sites. Mutation of a (-346, -333), b (-301, -288), and c (+3, +16) sites, but not the d (+75, +88) site, partially attenuated the ZFP64-mediated enhancement of *CSF1* promoter reporter activity, whereas the combined mutation of the a, b, and c sites completely abolished its activity (Fig. 4L). Additionally, we further confirmed that ZFP64 bound to a, b, and c sites of the *CSF1* promoter region using a ChIP-qPCR assay (Fig. S6C).

Then, we investigated the possibility that CSF1 is a primary effector of ZFP64-mediated processes. CSF1 knockdown attenuated the levels of CD163 and CD206 (membrane proteins), *CD206, ARG-1, IL-10, and TGF-β* (mRNA), IL-10 and TGF-β (secreted proteins), and the chemotactic migration of macrophages induced by $ZFP64^{high}$ HCC cells (Fig. 4M–P and S6D). These results indicate that ZFP64 promotes macrophage recruitment and M2-like polarization largely through the transcriptional activation of CSF1.

analysis of ChIP-sequencing and RNA-sequencing. Black curve, static background; red curve, activating function; blue curve, repressive function. (F) Venn diagram of overlapping genes between ChIP-sequencing and RNA-sequencing. (G) Enrichment of ZFP64 in the promoter region of *CSF1* according to ChIP-sequencing. (H–J) qRT-PCR, immunoblotting, and ELISA were used for detecting CSF1 expression. (K) Relative luciferase activities of reporters containing full-length or fragments of the *CSF1* promoter. (L) Relative luciferase activities of different reporters containing mutated sequences of the *CSF1* promoter in the indicated cells. Filled circles represent the putative ZFP64-binding sites, whereas "X" marks the mutated ZFP64-binding sites. The red letters of each binding region indicate putative or mutated ZFP64-binding sequences. (M) Quantification of CD163 and CD206 expression in macrophages using FCM analysis. (N) *CD206, ARG1, IL-10,* and *TGF-β* mRNA levels in macrophages, detected by qRT-PCR analyses. (O) Secreted IL-10 and TGF-β in macrophage supernatants, detected using ELISA. (P) Chemotactic migration assays of macrophages cocultured with HCC cells. ChIP, chromatin immunoprecipitation; FCM, flow cytometry; HCC, hepatocellular carcinoma; M, mutant; P, putative ZFP64-binding site; qRT-PCR, quantitative reverse-transcription PCR; WT, wild-type. (This figure appears in color on the web.)

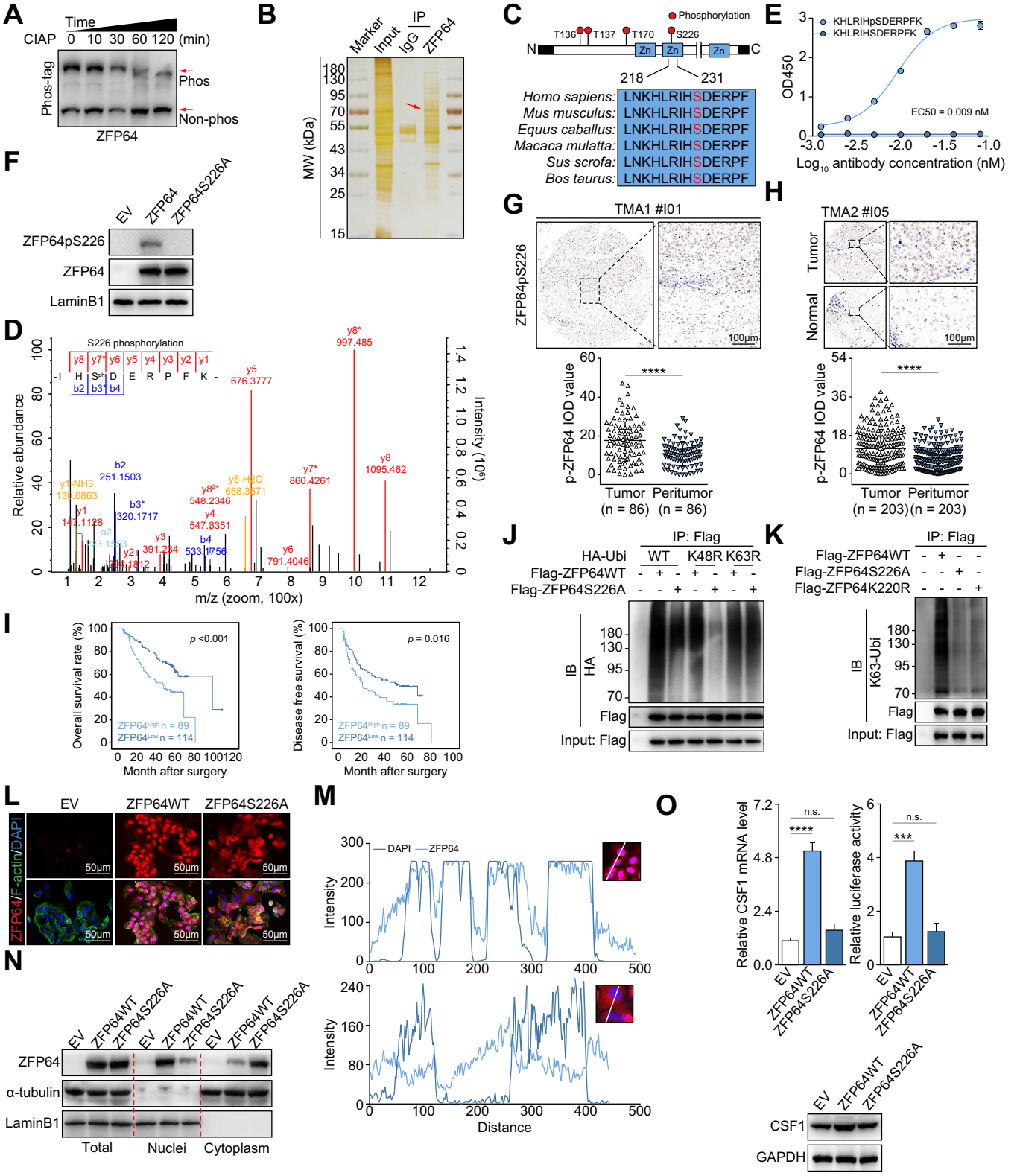

Fig. 5. S226 phosphorylation promotes ZFP64 nuclear translocation and CSF1 transcription. (A) Immunoblotting of proteins extracted from MHCC97H cells and subjected to Phos-tag™ SDS-PAGE. (B) IP was performed in MHCC97H cells and detection by silver staining. Red arrow shows the ZFP64 signal. (C) Schematic diagram showing the phosphorylation site of ZFP64 detected by LC-MS/MS (upper), and the ZFP64 amino acidic sequence near S226 from various species (lower). (D) LC-MS/MS spectrum showing the phosphorylation of ZFP64S226. (E) Detection of the specificity of the ZFP64pS226-specific antibody by ELISA. (F) Immunoblotting validation of ZFP64S226 phosphorylation in ZFP64-knockout MHCC97H cells after transfection with ZFP64WT or ZFP64S226A plasmids. (G-H) Detection of ZFP64pS226 levels in HCC tissues from TMA1 (G) and TMA2 (H) by IHC staining. (I) OS and DFS curves based on ZFP64pS226 levels. (J–K) MHCC97H cells were transfected with the indicated plasmids, immunoprecipitated using a Flag antibody, and then subjected to immunoblotting. (L) MHCC97H-sgZFP64

S266 phosphorylation promotes the K63-linked ubiquitination and nuclear translocation of ZFP64

ZFP64 is subjected to phosphorylation modifications, among which S266 is reported most frequently.[11,18,19] Herein, we performed immunoblotting using phosphate-affinity SDS-PAGE (Phos-tag^{TM}), and found that ZFP64 had an additional slow-migrating signal, which was gradually weakened in a time-dependent manner after calf intestinal alkaline phosphatase (CIAP) treatment (Fig. 5A). We then employed immunoprecipitation and liquid chromatography-tandem mass spectrometry (LC-MS/MS) to identify the phosphorylation sites of ZFP64 (Fig. 5B); we detected 4 phosphorylation sites (Fig. 5C, upper). Among them, S226 was located at the second zinc finger domain of ZFP64, and the amino acid sequence near S226 (LNKHLRIHS-DERPF) was highly conserved across species (Fig. 5C–D).

We generated an antibody that specifically recognized the phosphorylated ZFP64S226 (KHLRIHpSDERPFK) and tested its purity and specificity (Fig. 5E and S7A–B). Phosphorylated antibody detected signals in *ZFP64*-knockout MHCC97H cells transfected with the wild-type *ZFP64* (ZFP64WT) plasmid, but not the mutated *ZFP64* plasmid (ZFP64S226A) (Fig. 5F). Additionally, immunohistochemistry staining showed that phosphorylated ZFP64S226 was primarily present in the nuclei of HCC cells and significantly elevated in tumor tissues compared with those in paired normal tissues (Fig. 5G–H). Importantly, ZFP64pS226^{high} patients had shorter OS and disease-free survival than those with ZFP64pS226^{low} (Fig. 5I).

Interestingly, a recent study reported that ZFP64 is ubiquitinated at the K220 site, which is close to S226.[20] We speculated that S226 phosphorylation might affect ZFP64 ubiquitination. ZFP64 phosphorylation level was decreased after transfection with the flag-ZFP64S226A plasmid, while this phosphorylation level was abrogated in cells transfected with mutated K63-ubiquitin (K63R), but not K48R (Fig. 5J). We further confirmed this result by using a K63-specific ubiquitin antibody (Fig. 5K).

K63-linked ubiquitination might affect transcription factors' subcellular localization and transcriptional activity.[21,22] Interestingly, we found that ZFP64S226A was mainly present in the cytoplasm (Fig. 5L-M). By checking the levels of ZFP64 in the cytoplasmic and nuclear extracts, we further confirmed that the S226A mutation is associated with the reduced nuclear translocation of ZFP64 (Fig. 5N). Predictably, we found that the transcription and the expression levels of CSF1 were decreased in cells transfected with ZFP64S226A plasmid (Fig. 5O). These results indicate that the dephosphorylation of S226 inhibits the nuclear translocation and transcriptional activity of ZFP64.

The identified PKCα/ZFP64/CSF1 axis induces a suppressive TIME

To identify the protein kinase, we performed co-immunoprecipitation and LC-MS/MS. After removing the proteins shared by the IgG groups, we took an intersection and obtained a total of 97 proteins, 9 of which were kinases (Fig. 6A). Among them, protein kinase C alpha (PKCα) was highly expressed and activated in HCC tissues (Fig. S8A–B), and contained the putative motif (R-X-X-S/T) that phosphorylated ZFP64S226.[22] Using confocal immunofluorescence imaging, we found that ZFP64 and PKCα were colocalized in HCC cells (Fig. 6B and S9A–B). Co-immunoprecipitation results indicated the association between ZFP64 and PKCα (Fig. 6C and S10C). Importantly, GST pull-down assays demonstrated that *in vitro*-translated PKCα protein was pulled down by purified GST-ZFP64 fusion protein (Fig. 6D). Furthermore, we found that the zinc finger domain of ZFP64 (Δ141-447aa) is sufficient to bind PKCα, whereas PKCα interacted with ZFP64 through its Δ336-597aa and Δ598-672aa fragments (Fig. 6E). Then we generated a computational 3D complex structural model based on the X-ray crystal structure. Docking simulation data demonstrated that multiple amino acids in Δ141–447aa of ZFP64 and in Δ336–597aa and Δ598–672aa of PKCα may be responsible for their interaction (Fig. 6F).

Next, we performed an *in vitro* kinase assay, and confirmed that PKCα directly phosphorylated GST-ZFP64 *in vitro*, whereas this was abrogated by CIAP (Fig. 6G). We also noticed that following transfection with small-interfering RNA targeting PKCα (siPKCα), ZFP64pS226 levels were reduced (Fig. 6H). In contrast, levels of ZFP64pS226 and CSF1 were increased after treatment with PMA (an activator of PKCα), while these were reversed following transfection with siPKCα or siZFP64 (Fig. 6I).

Clinically, we observed positive correlations between PRKCA or ZFP64 and CSF1 in the TCGA cohort (Fig. S10A–B). In TMA2, high levels of p-PKCα, p-ZFP64, and CSF1 occurred frequently and concomitantly, and the overactivated PKCα/ZFP64/CSF1 axis often induced an immunosuppressive microenvironment in HCC (Fig. 6J). Additionally, a retrospective evaluation of the discovery cohort revealed that patients with PD had an overactivated PKCα/ZFP64/CSF1 axis and suppressive TIME compared to those with SD and PR (Fig. 6K-L). A highly activated PKCα/ZFP64/CSF1 axis, especially of p-ZFP64, was positively correlated with poor anti-PD1 treatment efficacy (Fig. 6M-N). These results indicate that the identified PKCα/ZFP64/CSF1 axis is positively correlated with poor efficacy of anti-PD1 treatment.

Gö6976 improves the TIME and anti-PD1 efficacy by targeting the PKCα/ZFP64/CSF1 axis

We further introduced Gö6976, an inhibitor of PKCα. The cell viability of MHCC97H was attenuated after Gö6976 treatment, exhibiting an IC50 of 25.41 μM (Fig. S11A). Importantly, we found that Gö6976 inhibited the activation of the PKCα/ZFP64/CSF1 axis in a dose- and time-dependent manner, and decreased the membrane-localized PKCα and nuclear-localized ZFP64 (Fig. 7A–C).

cells were transfected with the indicated plasmids, and IF was performed. (M) Fluorescence signal quantification according to the location of ZFP64 in (L). (N) Immunoblotting of nuclear and cytoplasmic extracts of MHCC97H-sgZFP64 cells transfected with ZFP64WT or ZFP64S226A plasmids. LaminB1 and α-tubulin were used as nuclear and cytoplasmic controls, respectively. (O) qRT-PCR, luciferase reporter gene, and immunoblotting assays were used to detect CSF1 expression in indicated cells. DFS, disease-free survival; HCC, hepatocellular carcinoma; IF, immunofluorescence; IHC, immunohistochemistry; IP, immunoprecipitation; LC-MS/MS, liquid chromatography-tandem mass spectrometry; OS, overall survival; PD, progressive disease; PR, partial response; qRT-PCR, quantitative reverse-transcription PCR; WT, wild-type. (This figure appears in color on the web.)

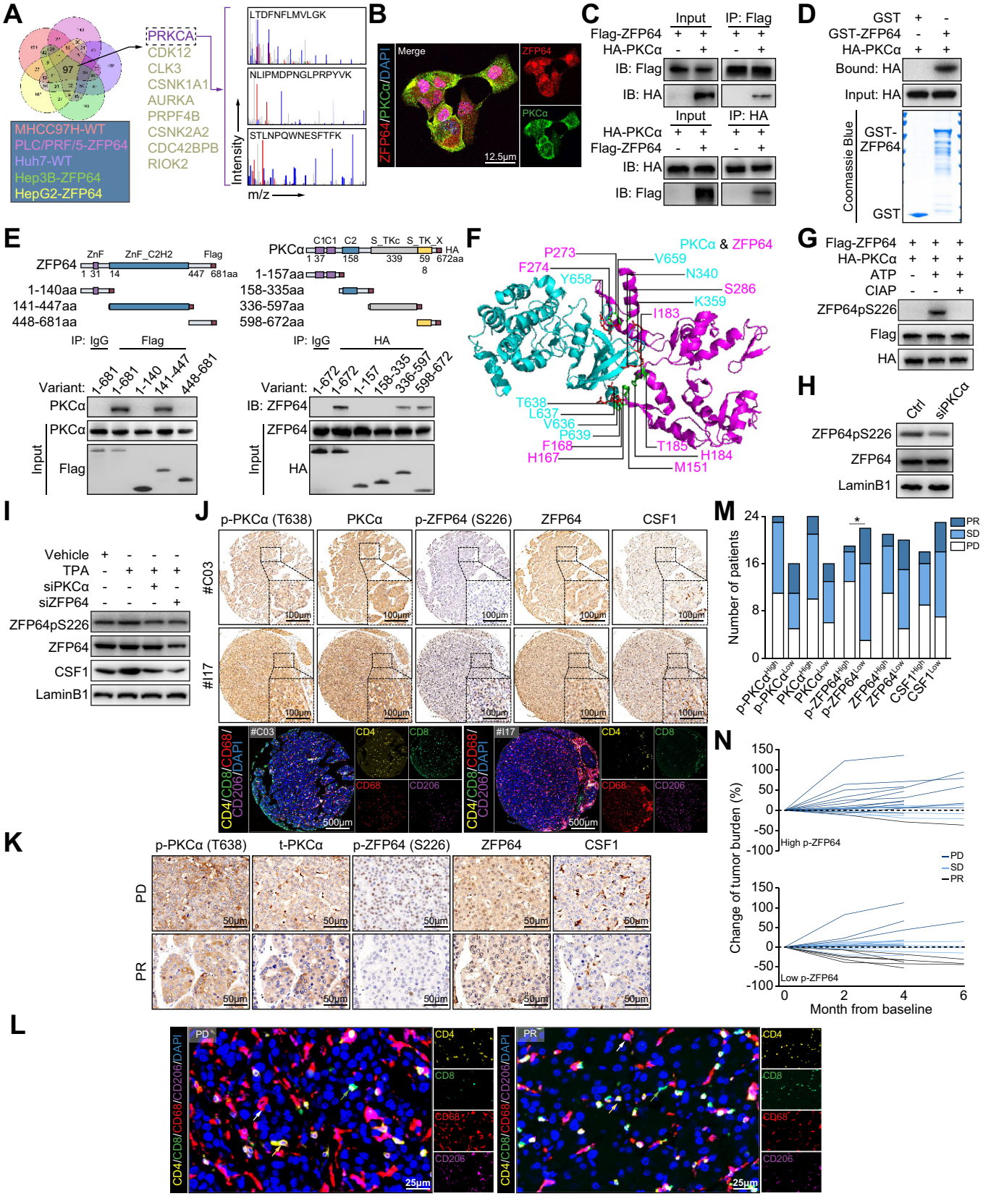

Fig. 6. The identified PKCα/ZFP64/CSF1 axis induces a suppressive TIME. (A) ZFP64-interacting proteins were identified using mass spectrometry. Venn diagram was used to identify the overlapping proteins in indicated cells. (B) Colocalization of ZFP64 and PKCα in MHCC97H cells detected by IF analysis. (C) Co-IP of endogenous ZFP64 and PKCα in MHCC97H cells after transfection with the indicated plasmids. (D) GST pull-down assay showing the direct interaction between

Using patient-derived xenograft and orthotopic xenograft tumor models, we showed that tumor weights in the Gö6976-treated group were significantly lower than those in the vehicle group (Fig. 7D and 7F). Decreased p-PKCα, p-ZFP64, CSF1, nuclear-localized ZFP64 levels, decreased F4/80$^+$ and CD206$^+$ cells, and increased CD4$^+$, CD8$^+$, and apoptotic cells were shown in the Gö6976-treated group compared with those in the vehicle group (Fig. 7E, 7G-H, and S11B-D). However, Gö6976-induced tumor inhibition and immune improvement were reversed by intraperitoneal administration of recombinant mouse CSF1 (Fig. S12A–B).

We then speculated that blocking the PKCα/ZFP64/CSF1 axis might improve anti-PD1 efficacy. To verify this, Gö6976 and another inhibitor, BLZ945 (targeting CSF1R), were introduced to block the PKCα/ZFP64/CSF1 axis. We found that in Hepa1-6-EV groups, Gö6976, BLZ945, anti-PD1, Gö6976 or BLZ945 combined with anti-PD1 inhibited tumor growth; while in Hepa1-6-ZFP64 groups, anti-PD1 could not inhibit, Gö6976 or BLZ945 partially inhibited, and Gö6976 or BLZ945 combined with anti-PD1 significantly inhibited tumor growth (Fig. 7I-N). Accordingly, we found that the combinational therapy evidently improved the TIME, as seen by the increased number of CD4$^+$ and CD8$^+$ cells and the decreased number of F4/80$^+$ and CD206$^+$ cells, especially in the ZFP64 overexpression group (Fig. S13A–D). We did not observe changes in body weights or significant side effects in these mice (Fig. S13E). Additionally, we developed an orthotopic xenograft tumor model and recorded the survival time of the mice, which further confirmed the aforementioned results (Fig. S13F–I).

Studies have reported that instead of sorafenib, lenvatinib partially inhibited tumor progression by reshaping the TIME.[23,24] In particular, lenvatinib was reported to decrease PKC expression, while sorafenib did not.[25] Herein, we found that only lenvatinib inhibited the PKCα/ZFP64/CSF1 axis, and this inhibition disappeared in siPKCα cells (Fig. S14A–C). Using *in vivo* assays, we observed that both lenvatinib and sorafenib inhibited tumor progression, but only lenvatinib specifically improved the TIME (Fig. S14D–E). Additionally, lenvatinib and anti-PD1 exerted synergistic antitumor effects and significantly prolonged the survival time of tumor-bearing mice (Fig. S14F–H). A combination of Gö6976 or lenvatinib with anti-PD1 showed no difference in therapeutic efficacy in ZFP64-overexpressing xenograft tumors (Fig. S14I–J). These findings indicate that lenvatinib reshapes the TIME partially through the identified PKCα/ZFP64/CSF1 axis, and that in treating ZFP64-overexpressing HCC, Gö6976 is as effective as lenvatinib in the anti-PD1 combinatorial scheme.

Discussion

Despite its successful application in multiple solid tumors, anti-PD1 therapy has benefited only a fraction of patients with HCC. In this study, we demonstrated that elevated ZFP64 was closely correlated with the anti-PD1 tolerance and the dismal prognosis of patients with HCC. Specifically, we found that PKCα phosphorylates ZFP64 at S226 and promotes its nuclear translocation, thereby transcriptionally activating CSF1. This process further induces the recruitment and M2-like polarization of macrophages, inducing immune escape and anti-PD1 tolerance. Clinically, patients with an activated PKCα/ZFP64/CSF1 axis frequently exhibited anti-PD1 resistance.

Multiple studies suggest that ZFP64 may accelerate tumor progression, but the exact function remains unclear.[14,16] We confirmed that ZFP64 promoted tumor progression and reflected poor prognosis in patients with HCC. Remarkably, we first demonstrated that high ZFP64 levels induced an immunosuppressive microenvironment. CSF1 is a central cytokine that regulates monocyte/macrophage differentiation, survival, and proliferation and promotes their recruitment and polarization.[26] We confirmed that ZFP64 transcriptionally regulated CSF1 expression by directly binding to its promoter region, and that secreted CSF1 strongly induced M2 polarization of recruited macrophages, thereby inducing an inhibitory TIME and promoting tumor progression. M2 macrophages play crucial roles in immune escape and ICB therapy resistance.[7,8] A recent study has demonstrated that patients with high levels of M2 infiltration tended to be resistant to anti-PD1 treatment.[27] Additionally, CSF1 also promotes tumor progression by activating multiple signals through the receptor CSF1R expressed by tumor cells.[28,29] Taken together, we demonstrate that the ZFP64/CSF1 axis is a powerful driver of tumor progression and anti-PD1 resistance in HCC.

Herein, we discovered that PKCα, an important protein kinase, directly complexed with ZFP64 and phosphorylated it at S226, promoting its nuclear translocation and the transcriptional activation of target genes. Clinically, high levels of p-PKCα, p-ZFP64, and CSF1 occurred frequently and concomitantly, and the overactivated PKCα/ZFP64/CSF1 axis often induced an immunosuppressive microenvironment. We also observed positive correlations between constituents of the PKCα/ZFP64/CSF1 axis and anti-PD1 efficacy, though most of these correlations were not statistically different, probably due to our limited sample size. We further introduced Gö6976, a classic inhibitor of PKCα, which has been previously shown to inhibit the progression of several tumors. For example, Gö6976 treatment 2 days after tumor implantation prevented 92% of tumor formation, whereas treatment 7 weeks after implantation caused complete regression of

ZFP64 and PKCα, and Coomassie blue staining showing the levels of GST-ZFP64 fusion protein. (E) Co-IP was performed in MHCC97H cells after transfection with indicated plasmids. (F) The crucial amino acids for the interaction between ZFP64 and PKCα were predicted using 3D structures. (G) Detection of ZFP64 phosphorylation by an *in vitro* kinase assay. (H) Immunoblotting detected ZFP64pS226 levels after transfection with indicated plasmids. (I) Immunoblotting showing protein levels in MHCC97H cells after transfection with the indicated plasmids. (J) IHC and mIF of indicated antibodies were performed in TMA2. (K) IHC was performed in the training cohort. (L) mIF analyses were performed in the training cohort, and representative images are presented. Green arrows (CD8$^+$ cells), yellow arrows (CD4$^+$ cells), white arrows (CD68$^+$CD206$^+$ cells). (M) Patients were categorized into high and low groups according to p-PKCα, PKC, p-ZFP64, ZFP64, and CSF1 levels; a correlation analysis of their levels and the efficacy of anti-PD1 treatment was performed. (N) Patients were categorized into high and low groups according to the p-ZFP64 level in tumor tissues; a fold line diagram was used to detect the changes in tumor size in patients with HCC after anti-PD1 treatment. HCC, hepatocellular carcinoma; IF, immunofluorescence; IHC, immunohistochemistry; mIF, multiplex immunofluorescence; TIME, tumor immune microenvironment. (This figure appears in color on the web.)

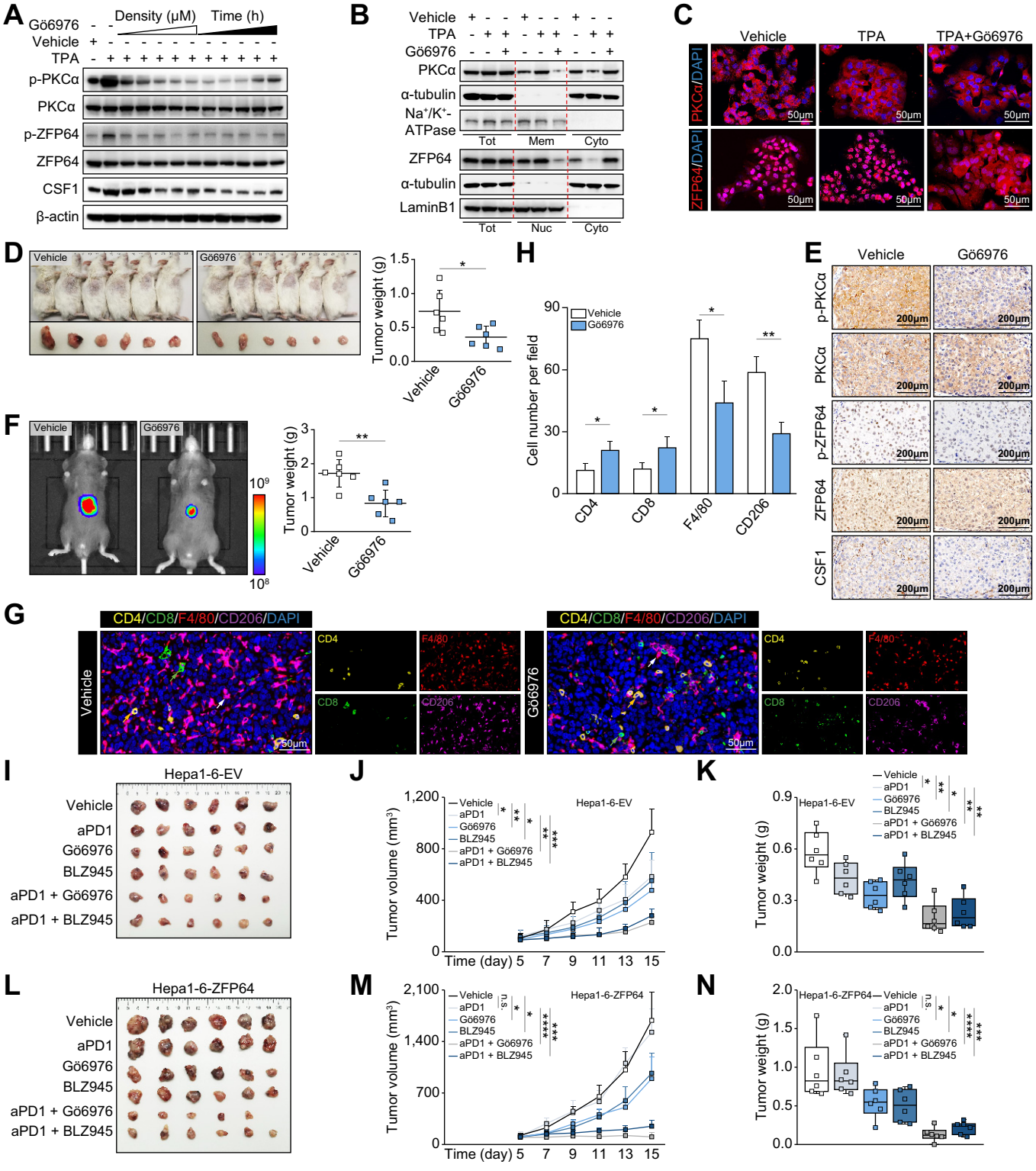

Fig. 7. Gö6976 improves the TIME and enhances anti-PD1 efficacy by inhibiting the PKCα/ZFP64/CSF1 axis. (A) Immunoblotting was performed in MHCC97H cells. (B) Immunoblotting of nuclear and membrane extracts (upper panel) or nuclear and cytoplasmic extracts (lower panel) of MHCC97H cells. (C) IF images of MHCC97H cells with indicated treatment. (D) NSG mice bearing PDX tumors were administered Gö6976 or vehicle, and tumor weights were measured at the endpoint. (E) IHC was performed in Gö6976- or vehicle-treated PDX tumor tissues. (F) Bioluminescence images of orthotopic HCC tumors at the endpoint. (G-H) Representative IF images of HCC tumor sections. Green arrows ($CD8^+$ cells), yellow arrows ($CD4^+$ cells), white arrows ($CD68^+CD206^+$ cells). (I–N) Hepa1-6-EV and Hepa1-6-ZFP64 cells were subcutaneously injected into C57BL/6 mice. When tumors reached 80–130 mm^3, mice were treated with anti-PD1, Gö6976, BLZ945, or a combination. Tumor volumes and weights were measured at indicated times. EV, empty vector; HCC, hepatocellular carcinoma; IF, immunofluorescence; IHC, immunohistochemistry; PDX, patient-derived xenograft; TIME, tumor immune microenvironment. (This figure appears in color on the web.)

established tumors.[30] We revealed that Gö6976 suppressed tumor progression and altered the TIME via the PKCα/ZFP64/CSF1 axis in HCC. Importantly, we presented extensive evidence that the combined treatment of Gö6976 with anti-PD1 could synergistically improve the survival of tumor-bearing mice, especially in those with ZFP64-overexpressing HCC.

In summary, we determined that the PKCα/ZFP64/CSF1 axis favors an inhibitory TIME by promoting M2-like polarization in recruited macrophages, and Gö6976 reshapes the tumor microenvironment and reverses anti-PD1 resistance. Our study reveals a promising therapeutic regimen for combination therapy with anti-PD1.

Abbreviations

CSF1, macropahge colony-stimulating factor; ZFP64, zinc finger protein 64; ChIP, chromatin immunoprecipitation; CR, complete response; CyTOF, mass cytometry by time of flight; DEGs, differentially expressed genes; EV, empty vector; FCM, flow cytometry; HCC, hepatocellular carcinoma; ICB, immune checkpoint blockade; LC-MS/MS, liquid chromatograpy tandem mass spectrometry; MRI, magnetic resonance imaging; OS, overall survival; PD, progressive disease; PD1, programmed cell death 1; PD-L1, programmed cell death ligand 1; PKCα, protein kinase C alpha; PMA, phorbol-12-myristate-13-acetate; PR, partial response; SD, stable disease; TAMs, tumor-associated macrophages; TCGA, The Cancer Genome Atlas; TIME, tumor immune microenvironment; t-SNE, t-distributed stochastic neighbor embedding; ZFP64, zinc finger protein 64.

Financial support

This work was funded by the National Natural Science Foundation of China (81972559, 81672825, and 81602513), the Shanghai Municipal Natural Science Foundation (21ZR1412200), the Clinical Research Plan of SHDC (SHDC2020CR2067B), the Chen Guang Program of Shanghai Municipal Education Commission (CJB), and the Young Elite Scientists Sponsorship Program by CAST (2019QNRC001).

Conflicts of interest

The authors have declared no conflict of interest.

Please refer to the accompanying ICMJE disclosure forms for further details.

Authors' contributions

JF, AK, JC designed and conceived this project. CW, MZ and PZ performed experiments, analyzed data, and wrote the manuscript. JW, RP, XY, CG, JG, SW, YZ, ZT analyzed and interpreted data. XY, ZH, XC generated reagents. CW, MZ, PZ and XH analyzed the data and collected tumor samples. JF, AK, JC QG, JZ supervised the study. All authors contributed to and approved the manuscript.

Data availability statement

The data used to support the findings of this study are included and available within the article.

Supplementary data

Supplementary data to this article can be found online at https://doi.org/10.1016/j.jhep.2022.02.019.

References

Author names in bold designate shared co-first authorship.

[1] Llovet JM, Kelley RK, Villanueva A, Singal AG, Pikarsky E, Roayaie S, et al. Hepatocellular carcinoma. Nat Rev Dis Primers 2021;7:6.
[2] Dang H, Takai A, Forgues M, Pomyen Y, Mou H, Xue W, et al. Oncogenic activation of the RNA binding protein NELFE and MYC signaling in hepatocellular carcinoma. Cancer Cell 2017;32.
[3] Eggermont AMM, Blank CU, Mandala M, Long GV, Atkinson V, Dalle S, et al. Adjuvant pembrolizumab versus placebo in resected stage III melanoma. N Engl J Med 2018;378:1789–1801.
[4] Finn RS, Ryoo B-Y, Merle P, Kudo M, Bouattour M, Lim HY, et al. Pembrolizumab as second-line therapy in patients with advanced hepatocellular carcinoma in KEYNOTE-240: a randomized, double-blind, phase III trial. J Clin Oncol 2020;38:193–202.
[5] D'Alessio A, Cammarota A, Prete MG, Pressiani T, Rimassa L. The evolving treatment paradigm of advanced hepatocellular carcinoma: putting all the pieces back together. Curr Opin Oncol 2021;33:386–394.
[6] **MacParland SA**, **Liu JC**, **Ma X-Z**, Innes BT, Bartczak AM, Gage BK, et al. Single cell RNA sequencing of human liver reveals distinct intrahepatic macrophage populations. Nat Commun 2018;9:4383.
[7] **Xiao H**, **Guo Y**, **Li B**, Li X, Wang Y, Han S, et al. M2-Like tumor-associated macrophage-targeted codelivery of STAT6 inhibitor and IKKβ siRNA induces M2-to-M1 repolarization for cancer immunotherapy with low immune side effects. ACS Cent Sci 2020;6:1208–1222.
[8] DeNardo DG, Ruffell B. Macrophages as regulators of tumour immunity and immunotherapy. Nat Rev Immunol 2019;19:369–382.
[9] Wang Y, Tiruthani K, Li S, Hu M, Zhong G, Tang Y, et al. mRNA delivery of a bispecific single-domain antibody to polarize tumor-associated macrophages and synergize immunotherapy against liver malignancies. Adv Mater 2021;33:e2007603.
[10] Goswami S, Walle T, Cornish AE, Basu S, Anandhan S, Fernandez I, et al. Immune profiling of human tumors identifies CD73 as a combinatorial target in glioblastoma. Nat Med 2020;26:39–46.
[11] Mack HG, Beck F, Bowtell DD. A search for a mammalian homologue of the Drosophila photoreceptor development gene glass yields Zfp64, a zinc finger encoding gene which maps to the distal end of mouse chromosome 2. Gene 1997;185:11–17.
[12] Wang D, Zhu Z-Z, Jiang H, Zhu J, Cong W-M, Wen B-J, et al. Multiple genes identified as targets for 20q13.12-13.33 gain contributing to unfavorable clinical outcomes in patients with hepatocellular carcinoma. Hepatol Int 2015;9:438–446.
[13] Li S-Y, An P, Cai H-Y, Bai X, Zhang Y-N, Yu B, et al. Proteomic analysis of differentially expressed proteins involving in liver metastasis of human colorectal carcinoma. Hepatobiliary Pancreat Dis Int 2010;9:149–153.
[14] Lu B, Klingbeil O, Tarumoto Y, Somerville TDD, Huang Y-H, Wei Y, et al. A transcription factor Addiction in leukemia imposed by the MLL promoter sequence. Cancer Cell 2018;34.
[15] Seymour L, Bogaerts J, Perrone A, Ford R, Schwartz LH, Mandrekar S, et al. iRECIST: guidelines for response criteria for use in trials testing immunotherapeutics. Lancet Oncol 2017;18:e143–e152.
[16] Jiang J, Zhang J, Fu K, Zhang T. Function and mechanism exploration of zinc finger protein 64 in lung adenocarcinoma cell growth and metastasis. J Recept Signal Transduct Res 2020:1–9.
[17] Galli A, Ceni E, Mello T, Polvani S, Tarocchi M, Buccoliero F, et al. Thiazolidinediones inhibit hepatocarcinogenesis in hepatitis B virus-transgenic mice by peroxisome proliferator-activated receptor gamma-independent regulation of nucleophosmin. Hepatology 2010;52:493–505.
[18] **Mertins P**, **Mani DR**, **Ruggles KV**, **Gillette MA**, Clauser KR, Wang P, et al. Proteogenomics connects somatic mutations to signalling in breast cancer. Nature 2016;534:55–62.
[19] Mertins P, Qiao JW, Patel J, Udeshi ND, Clauser KR, Mani DR, et al. Integrated proteomic analysis of post-translational modifications by serial enrichment. Nat Methods 2013;10:634–637.
[20] Akimov V, Barrio-Hernandez I, Hansen SVF, Hallenborg P, Pedersen A-K, Bekker-Jensen DB, et al. UbiSite approach for comprehensive mapping of lysine and N-terminal ubiquitination sites. Nat Struct Mol Biol 2018;25:631–640.
[21] Erpapazoglou Z, Walker O, Haguenauer-Tsapis R. Versatile roles of k63-linked ubiquitin chains in trafficking. Cells 2014;3:1027–1088.

[22] Pearson RB, Kemp BE. Protein kinase phosphorylation site sequences and consensus specificity motifs: tabulations. Methods Enzymol 1991;200:62–81.
[23] **Kimura T**, **Kato Y**, Ozawa Y, Kodama K, Ito J, Ichikawa K, et al. Immunomodulatory activity of lenvatinib contributes to antitumor activity in the Hepa1-6 hepatocellular carcinoma model. Cancer Sci 2018;109:3993–4002.
[24] Kato Y, Tabata K, Kimura T, Yachie-Kinoshita A, Ozawa Y, Yamada K, et al. Lenvatinib plus anti-PD-1 antibody combination treatment activates CD8+ T cells through reduction of tumor-associated macrophage and activation of the interferon pathway. PLoS One 2019;14:e0212513.
[25] Kim S-M, Kim SY, Park CS, Chang H-S, Park KC. Impact of age-related genetic differences on the therapeutic outcome of papillary thyroid cancer. Cancers (Basel) 2020;12.
[26] Neubert NJ, Schmittnaegel M, Bordry N, Nassiri S, Wald N, Martignier C, et al. T cell-induced CSF1 promotes melanoma resistance to PD1 blockade. Sci Transl Med 2018;10.
[27] **Zhu Y**, **Yang J**, **Xu D**, **Gao X-M**, **Zhang Z**, Hsu JL, et al. Disruption of tumour-associated macrophage trafficking by the osteopontin-induced colony-stimulating factor-1 signalling sensitises hepatocellular carcinoma to anti-PD-L1 blockade. Gut 2019;68:1653–1666.
[28] Espinosa I, Beck AH, Lee C-H, Zhu S, Montgomery KD, Marinelli RJ, et al. Coordinate expression of colony-stimulating factor-1 and colony-stimulating factor-1-related proteins is associated with poor prognosis in gynecological and nongynecological leiomyosarcoma. Am J Pathol 2009;174:2347–2356.
[29] Lemmon MA, Schlessinger J. Cell signaling by receptor tyrosine kinases. Cell 2010;141:1117–1134.
[30] Biswas DK, Martin KJ, McAlister C, Cruz AP, Graner E, Dai S-c, et al. Apoptosis caused by chemotherapeutic inhibition of nuclear factor-kappaB activation. Cancer Res 2003;63:290–295.